Polydispersed Powders (Nd³⁺:YVO₄) for Ultra Efficient Random Lasers

Niklaus U. Wetter,* Julia M. Giehl, Felix Butzbach, Danilo Anacleto, and Ernesto Jiménez-Villar

Random lasers hold the potential for cheap, coherent light sources that can be miniaturized and molded into any shape with several other added benefits such as speckle-free imaging; however, they require improvements specifically in terms of efficiency. This paper details for the first time a strategy for increasing the efficiency of a random laser that consists in using smaller particles, trapped between large particles to serve as absorption and gain centers whereas the large particles control mainly the light diffusion into the sample. Measurements of backscattering cone, sample absorption, reflection, and laser emission are used to determine the samples' transport mean free path, fill fractions, laser efficiency, and the average photon path lengths inside the scattering medium for backscattered pump photons. A record slope efficiency of 50% is reached by optimizing pump photon diffusion and absorption in a powder pellet composed by a polydispersed particle size distribution (smaller particles between bigger ones) from a grinded and sieved 1.33 mol% yttrium vanadate doped with neodymium crystal with mean particle size of 54 µm.

1. Introduction

The possibility of generating stimulated emission in scattering media with gain (random laser) was historically proposed by Letokhov in the 1960s.[1,2] These lasers were experimentally demonstrated for the first time in 1993 by Gouedard et al.[3] A major advantage of random lasers over regular lasers is that their production is cheap, the required technology relatively simple and it is possible to produce random lasers with several different materials such as semiconductor nanoparticles,[4] ceramic powders and polymers,[5] organic materials, and biological tissues.[6,7] Potential applications such as speckle-free imaging in biology, remote sensing, display technology, encrypting, cancer detection, and distributed amplification, require optimization of random laser performance with respect to laser efficiency and, in some cases, also with respect to radiance, in order to obtain a useful, directional output beam.[8,9] Only when random lasers achieve efficiency comparable to traditional lasers will their inherent cost advantages become attractive for the large majority of applications.

In order to overcome the problems of random lasers associated to nondirectional output and lack of efficiency, the main approach has been to choose low-dimensional random lasers. 1D fiber random lasers are well suited for this purpose and have achieved up to several watts of continuous output.[10] 2D distributed feedback (DFB) lasers have demonstrated highly efficient and directional output in the microjoule range.[11] These low-dimensional random lasers are generally quite large (like in the case of random fiber lasers) and require sophisticated production methods that are in stark contrast to the simplicity and practicality of the 3D random laser production.

Noginov and co-workers have studied the dependence of random laser emission in neodymium doped powders (Nd$_{0.5}$La$_{0.5}$Al$_3$(BO$_3$)$_4$) on the particle size, the powder volume density, and the pump spot size.[12,13] Best reported efficiency was below half a percent. An impediment for increasing the efficiency is the surface reflectivity of the compacted powders. The bulk reflection coefficient of Nd$_{0.5}$La$_{0.5}$Al$_3$(BO$_3$)$_4$ at $\lambda = 532$ nm for medium to high powder density is ≈ 0.7.[13] Using a fiber-coupled random laser, where the pump fiber terminates deep inside the scattering medium in order to deliver the pump energy directly into the gain volume without reflection loss at the surface, Noginov et al. achieved a higher efficiency of $\approx 0.7\%$.[14] Azkargorta et al. achieved 20% and 42% slope efficiencies with respect to pump power using Nd: yttrium aluminium garnet (YAG) and Nd$_3$Ga$_5$O$_{12}$ crystal powders.[15,16]

The stimulated random laser (RL) emission of these rare earth doped powder pellets comes in the form of a Lambertian emission with a linewidth that decreases around laser threshold and becomes much smaller than typical amplified spontaneous emission (ASE).[17] Output power also shows a typical laser threshold and slope efficiency. As we have shown for yttrium vanadate doped with neodymium (Nd:YVO₄), the emission decay after a pump pulse follows two different exponentials corresponding to a fast laser emission decay of a few microseconds and a slower fluorescence emission decay which is shorter than the intrinsic decay time, which should amount to 73 µs for 1.33 mol% neodymium doping concentration, because of upconversion.[18] We therefore expected some decrease in laser efficiency due to energy transfer upconversion.

Dr. N. U. Wetter, Dr. J. M. Giehl, F. Butzbach, D. Anacleto,
Dr. E. Jiménez-Villar
Center for Lasers and Applications
Instituto de Pesquisas Energéticas e Nucleares IPEN-CNEN/SP
Av. Prof. Lineu Preses, 2242 São Paulo, SP, Brazil
E-mail: nuwetter@ipen.br

Table 1. Groups of powder grain size distributions for the monodispersed and polydispersed Nd^{3+}:YVO_4 powders measured by Fraunhofer laser diffraction technique. The size measurement of group B_5 was performed by SEM image, analyzing around 200 particles.

Mesh [µm]	Groups A polydispersed mean particle size		A—size at 10% volume fraction	SD	Groups B Monodispersed mean particle size		B—size at 10% volume fraction	SD
10–20	A_1	9.5 µm	0.87 µm	7.3	B_1	9.9 µm	0.61 µm	0.98
20–45	A_2	15 µm	0.95 µm	12	B_2	37 µm	16 µm	2.17
45–75	A_3	30 µm	1.05 µm	–	B_3	55 µm	17 µm	–
75–106	A_4	54 µm	6 µm	39	B_4	96 µm	31 µm	4.7
106–180	A_5	125 µm	30 µm	–	B_5	*147 µm	*113 µm	–

To further increase the efficiency of the random laser, we propose a system composed of mixed grains of different sizes, with smaller grains located in the spaces between larger particles. The system has high volume fraction of large grains, which we control by using different mesh sizes ranging from 10 to 180 µm, and a small volume fraction of much smaller grains. Although the volume fraction of these smaller grains is only a few percent, in terms of numbers they make up the majority of the particles. These small particles, which are trapped in between the big particles, create regions (pockets) with shorter transport mean free path and therefore concentrate the light. Consequently, the absorption mean free length within these pockets must be considerably smaller than within the bigger particles, therefore, these regions would serve as absorption and gain centers inside the random laser. Additionally, these pockets would be pumped by all sides and from any direction due to the light diffusion that would be governed by the bigger particles. This strategy of using smaller particles to fill the spaces between the larger particles opens a new technique to increase the efficiency of random lasers and differs from previous techniques that use codoping with other materials to improve the random laser performance.[19–21] Note that the coherent emission of the random laser, captured by the backscattering cone, originates from a volume that corresponds in depth to several times the transport mean free path. In this way, the pumped volume is basically determined by larger particles, which govern the macroscopic (averaged) diffusion properties of light inside the samples. By adjusting the volume fraction of each particle size we can control separately the mechanisms of gain and diffusion thereby optimizing the output efficiency of this new type of random laser. On the contrary, a random laser composed by a homogeneous scattering medium with short transport mean free path would be pumped only from the front side of the sample, reducing considerably the volume and intensity of pumping and, consequently, its efficiency. A promising method called fraction of absorbed pumping (FAP) was used to study the absorption and diffusion processes in the samples,[22–25] which allowed us to determine that the absorbance increases appreciably with the introduction of smaller grains between the big particles.
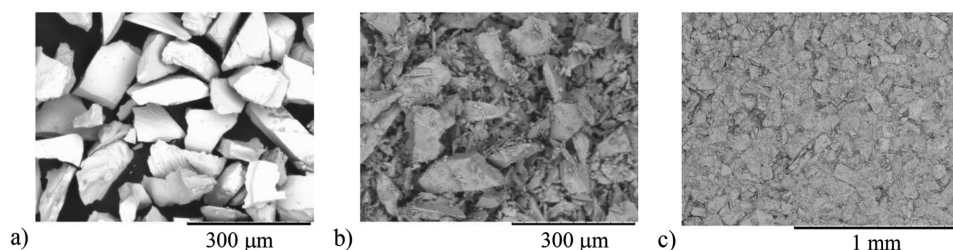
2. Sample Preparation and Experimental Setup

In a random laser, several cavity parameters are random or cannot be determined and therefore we concentrate on the controllable parameters, which are the absorption coefficient, gain coefficient, doping level, index of refraction, and transport mean free path. In order to achieve a powder with a high gain coefficient, necessary for highly efficient laser action, we used an Nd^{3+}:YVO_4 crystal, known for its excellent performance in diode pumped solid state lasers.[26] There are a series of other laser crystals which result in similar efficiencies when used in traditional standing wave cavities such as Nd:YAG and Nd:yttrium lithium fluoride (YLF).[27,28] However, Nd:YVO is a birefringent crystal with an average refractive index of 2.04 at the pump wavelength of 806.5 nm that is much higher when compared to the other high gain crystals and therefore suits our purpose of strong scattering. The typical absorption coefficient for Nd:YVO_4 is very high, 79 cm^{-1} (polarization along c-axis) and 17 cm^{-1} (polarization along other axes) for 1 mol% neodymium doping.[29] In order to further enhance the absorption we used a YVO crystal with 1.33 mol% neodymium doping, which results in a ballistic absorption coefficient of 50 cm^{-1} for the bulk crystal and for unpolarized light. Taking into account the spectral overlap efficiency between crystal absorption at 806 nm and the broad diode pump emission at this wavelength, an absorption coefficient of 39 cm^{-1} is determined, corresponding to a ballistic absorption length of 256 µm. Pieces of the Nd:YVO_4 crystal were grinded and the powder sieved by means of differently sized mesh grids to obtain ranges of different particle sizes (**Table 1**).

The mesh grids ranged from a 10 µm mesh to a 180 µm mesh. When observed beneath the microscope, the powders were not monodispersed. On the contrary, a large quantity of smaller particles adhered to the large particles retained by the sieve. The powders were separated into two groups, one group received no further treatments and the other one underwent a cleansing procedure with the objective to get better monodispersed powders. This last procedure consisted of mixing isopropyl alcohol with the powders, stirring the liquid mechanically for 5 min in ultrasound, then sieving the mixture again and drying for a period of 24 h. The result was satisfactory for the larger grain sizes, however, for a mesh size of 20 µm or less the procedure did not work properly and the powder still consisted of a mixture of large and small particles. A total of three powder samples were prepared for each group. Particle size dispersion was analyzed with the laser diffraction technique (Compagnie Industrielle des Lasers (CILAS)).

Table 1 shows the strong participation of smaller particles in the A groups when comparing their mean particle sizes with their monodispersed counterpart: in all cases the A groups show smaller mean diameters. Also clearly seen is the much larger standard deviation (SD) of the mixed groups

**ADVANCED
SCIENCE NEWS**
www.advancedsciencenews.com

Particle
& Particle Systems Characterization
www.particle-journal.com

Figure 1. SEM images of $Nd^{3+}:YVO_4$ powders from a) monodispersed (cleansed) samples and b) polydispersed samples. The images are from samples of group 4 (B_4 and A_4, respectively). Image (c) is from the surface of a pressed pellet from group A_4.

when compared to the cleansed groups. Main particle size of group B_5 was obtained by scanning electron microscopy (SEM) image analysis because the high quantity of large particles caused errors to the results produced by the CILAS equipment and because it is easier to count large monodispersed particles by SEM analysis. Additional information to the standard deviation of the powder distribution is the particle diameter at 10% of the cumulative population density, which quantifies well the participation of small particles in the samples. The column with the particle size at 10% in Table 1 gives the volume fraction of particles smaller than this size, e.g., 10% of the occupied volume in sample A_4 is of particles smaller than 6 µm. Examples of the powders are shown in **Figure 1**. In order to characterize the grain size distribution in each sample we used the Fraunhofer laser diffraction technique (model CILAS 930), which is appropriate, given the fact that our sieves retained mainly particles between 10 and 500 µm. The result of the analysis comes in the form of a table containing about 100 classes of different particle diameters and the respective population density. The average of three powder samples of each group was used to calculate the mean diameter and the standard deviation by means of a MATLAB program, which was also used to calculate the scattering cross-section and transport mean free path of each group.

In **Figure 2**a a histogram is shown for a sample of group B_2, where the symmetric distribution on a log scale around the mean value shows that the cleansing procedure works well whereas the respective polydispersed sample (A_2, Figure 2b) presents a higher percentage of small particles, demonstrated by the characteristic shoulder to the left of the histogram peak. Approximately 60 mg of powder were used to form pellets with

a diameter of 5 mm and of 1–1.5 mm thickness compacted at a pressure of 255 MPa.[30]

3. Absorption Measurements and Transport Mean Free Path Calculations

The absorption measurements of the pellets were accomplished with a spectrophotometer (Agilent, model Cary 5000) with integrating sphere. Reflectivity was measured at 705 nm (zero absorption of neodymium ions) and absorption was measured at 805 nm (absorption peak of neodymium) although the absorption peak could change slightly for each sample, most likely due to equipment instabilities (**Figure 3**a). Given the large ballistic absorption coefficient of 39 cm^{-1}, 87% of the pump radiation at this wavelength is absorbed within a depth of half a millimeter of bulk crystal. Notice that inside the pellets the absorption depth is smaller, determined by the macroscopic absorption length, which also depends on the fill fraction and the transport mean free path. It was experimentally verified by making transmission measurements with thin ($\approx$0.5 mm) pellets that all pump radiation is absorbed. Some of the large grain size pellets had to be handled very carefully and chipped easily.

The average reflectivity of the samples at 705 nm was between 80% and 90% (specular included). The reflection at the pellet surface (first surface) for an average index of refraction of 2.03 is 11% in the case of a dense pellet surface without a significant fraction of voids. In Figure 1c we can observe that the surface can be approximated by a mainly dense and flat surface with only a few voids. We therefore decreased the measured reflectivity values by 11% in order
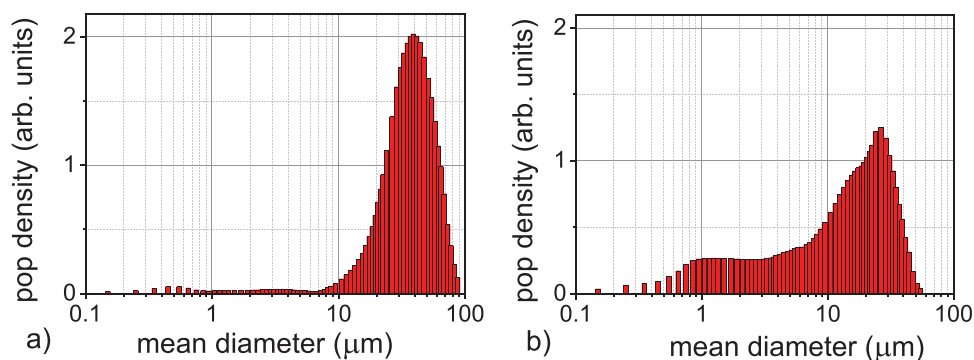
Figure 2. Histogram of population density in volume from a) a monodispersed sample of B_2 and b) a polydispersed sample of group A_2. Additional histograms of other groups can be found in the Supporting Information (Figure S1, Supporting Information).
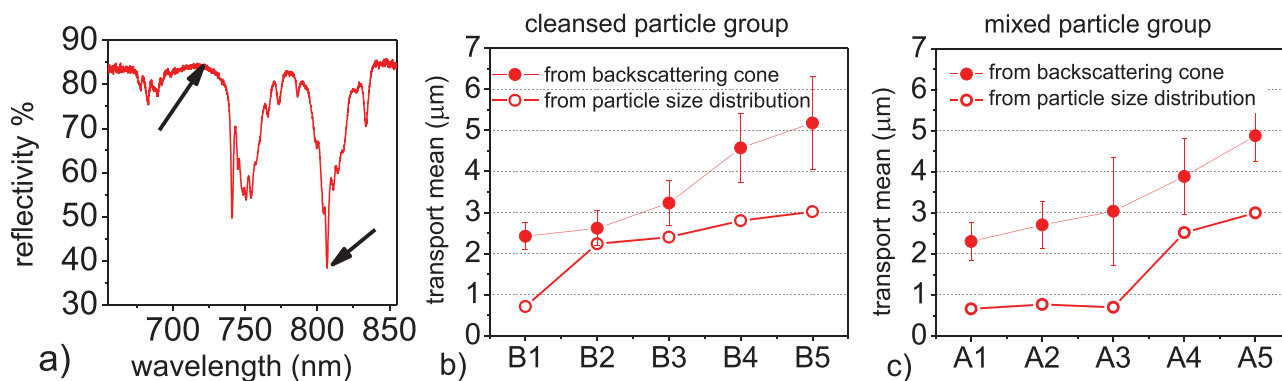
Figure 3. a) Typical absorption-reflection spectrum of a powder pellet (sample A$_4$). Arrows indicate minimum absorption (only reflection) at 705 nm and maximum absorption at 805 nm. Transport mean free path as obtained from backscattering cone measurements (closed circles) and calculated from particle size distribution (open circles) b) for monodispersed samples and c) for polydispersed samples.

to subtract the first surface reflection and calculate absorption. We designated the ratio between the pumping intensities reflected by the samples at 705 and 805 nm as the FAP. From the natural logarithm of FAP, we can estimate the average photon path length (l_c) inside the sample before being reflected (Equation (1))

$$FAP = \frac{I_{R(705\ nm)}}{I_{R(805\ nm)}} \Rightarrow \ln(FAP) \approx l_c/l_a \rightarrow l_c \approx l_a \times \ln(FAP) \tag{1}$$

where l_a is the microscopic absorption length. For the calculation we have considered that diffusion of light is approximately similar for these two wavelengths (705 and 806 nm). FAP values for each sample are shown in **Table 2**, given by the average of two measurement runs made on different days. In order to calculate l_c we need to know the microscopic absorption length l_a, which is the ballistic absorption length at 805 nm, $1/\alpha$ (256 µm) divided by the fill fraction (ff) that will be calculated in Section (5).

A setup for measuring the transport mean free path was installed, as shown in **Figure 4**a.[31] A 30 mW HeNe laser ($\lambda = 632.8$ nm) was first polarized in the vertical direction by a polarizer cube and its beam diameter was expanded to 5 mm in order to illuminate a larger area of the sample, which improves the resolution of the setup. A modified Michelson interferometer configuration was employed to detect the backscattered intensity coming from the sample. The sample is fixed on a motor rotating at a speed of ≈50 Hz in order to ensemble average the speckles

coming from the sample surface. The sample was tilted 15° in order to remove unwanted Fresnel reflections (more than 15° results in a change of the width of the backscattering cone). The backscattered light went through an analyzer, in order to measure the vertical polarization conserving channel. The backscattered light was focused onto a charge coupled device (CCD) camera using first an $f = 150$ mm and later an $f = 50$ mm lens. The use of two setups using different focusing lenses was to improve the precision of the measurement. The longer focal length gives higher precision for the center of the backscattering cone whereas the smaller focal length gives better precision for the wings of the backscattering cone. The images of the coherent backscattering cone were adjusted to a theoretical fit and the transport mean free path l_t, which is inversely proportional to the full width at half maximum (FWHM) of the fitted coherent backscattering (CBS) cone, was calculated from the following equation[32,33]

$$l_t = \frac{0.35 * \lambda}{2 \cdot \pi \cdot FWHM} \tag{2}$$

where the factor of 0.35 is a correction for the sample's internal reflection at 632 nm.[34,35] The results for the transport mean free path are shown in Figure 3b,c (closed circles). Also shown are the calculated results obtained from the particle distribution, measured with the Fraunhofer diffraction method, considering an ff equal unity (open circles). As expected, the polydispersed groups always show smaller transport mean free path, which is associated to the scattering increase provided by smaller particles.

Figure 3b,c shows, for both groups, a difference between l_t values obtained from backscattering cone and particle size distribution. The difference between both l_t curves is attributed to the filling factor, because our calculated l_t values results assume a filling factor of unity. The filling fraction given by this ratio is shown in Table 2. A much larger difference between both curves is observed whenever the calculated transport mean free path is below ≈1 µm, which occurs for groups B$_1$, A$_1$, A$_2$, and A$_3$. We attribute this effect to the following causes: (i) the presence of agglomerates of smaller particles (smaller than wavelength), such that the space between scattering surfaces is smaller than one wavelength. This should favor the near-field coupling,[36] which decreases the effective scattering strength.[22–24] (ii) The

Table 2. FAP values and filling fraction for the monodispersed (B) and polydispersed (A) samples. ff* is the fill fraction calculated from the particle distribution and ff** is the fill fraction calculated with Equation (4). *samples that probably contain agglomerates.
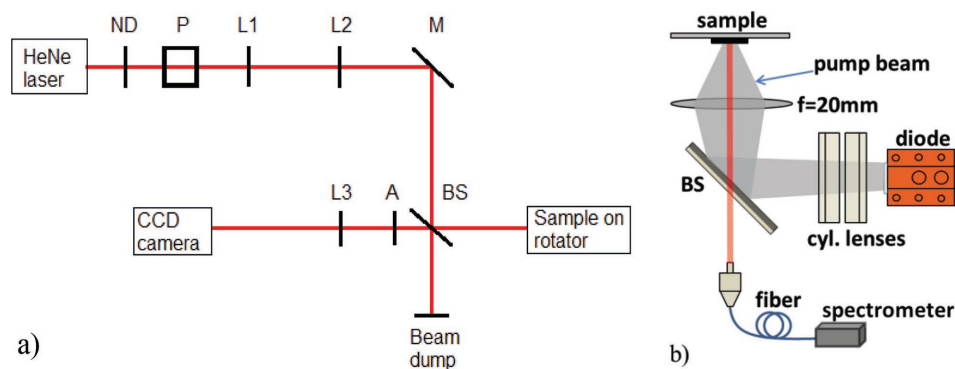
	Polydispersed				Monodispersed		
	FAP	ff*	ff**		FAP	ff*	ff**
A$_1$	1.78	0.28*	0.96	B$_1$	1.57	0.29*	0.91
A$_2$	1.9	0.28*	0.85	B$_2$	1.83	0.85	0.86
A$_3$	2.15	0.23*	0.78	B$_3$	2.09	0.74	0.74
A$_4$	2.42	0.64	0.66	B$_4$	2.34	0.61	0.61
A$_5$	2.55	0.61	0.59	B$_5$	2.23	0.58	0.57

**ADVANCED
SCIENCE NEWS**
www.advancedsciencenews.com

Particle
& Particle Systems Characterization
www.particle-journal.com

Figure 4. a) Setup used to measure coherent backscattering intensity profiles. ND is variable neutral density filter; P is a polarizer cube; M is a gold coated mirror; BS is a 50% beam splitter (632.8 nm); A is an analyzer; L1, L2, and L3 are lenses with focal lengths of 50, 200, and 50 mm (or 150 mm), respectively. b) Schematic of the setup used for measuring the linewidth narrowing of the random lasers. BS is the beam splitter and the cylindrical lenses have focal lengths of −13 and −25 mm.

agglomerates made of smaller particles should behave approximately like a bigger particle with a lower effective scattering cross-section (lower effective refractive index).

4. Laser Operation

The laser setup included a quasi-continuous (qcw), fast-axis-collimated laser diode bar, operating at 806.5 nm with 5 Hz repetition rate (Figure 4b). Two cylindrical divergent lenses with focal length of −13 and −25 mm were used for a modal conformation of the pump beam (beam parameters before conformation: $M_x^2 \approx 2000$ and $M_y^2 = 3$), such that by inserting an $f = 20$ mm spherical lens at 35 mm from the sample, a rectangular shaped focus of the excitation beam with total area of 3 mm² could be achieved at the samples surface. The maximum peak power of the square shaped pulse of 150 µs pulse width was 55 W at the sample's location corresponding to 8.2 mJ of pulse energy. The sample itself was mounted on a motor that was kept at a constant rotation of $\approx$20 Hz. The emission of the random laser in the form of a back-scattering cone was separated from the pump radiation by a beam splitter (BS) which was highly reflective for the pump radiation and had high transmission at the emission wavelength of 1064 nm. A pyroelectric energy sensor with resolution of 100 nJ (Thorlabs ES111C) was positioned at 12 cm from the beam splitter. It was verified that all emission captured by the spherical lens of one inch diameter was collected inside the detector area of 10 mm diameter. Further details about the shape of the pump spot or the shape of the random laser beam at the detector and its degree of coherence are given in ref. [18].
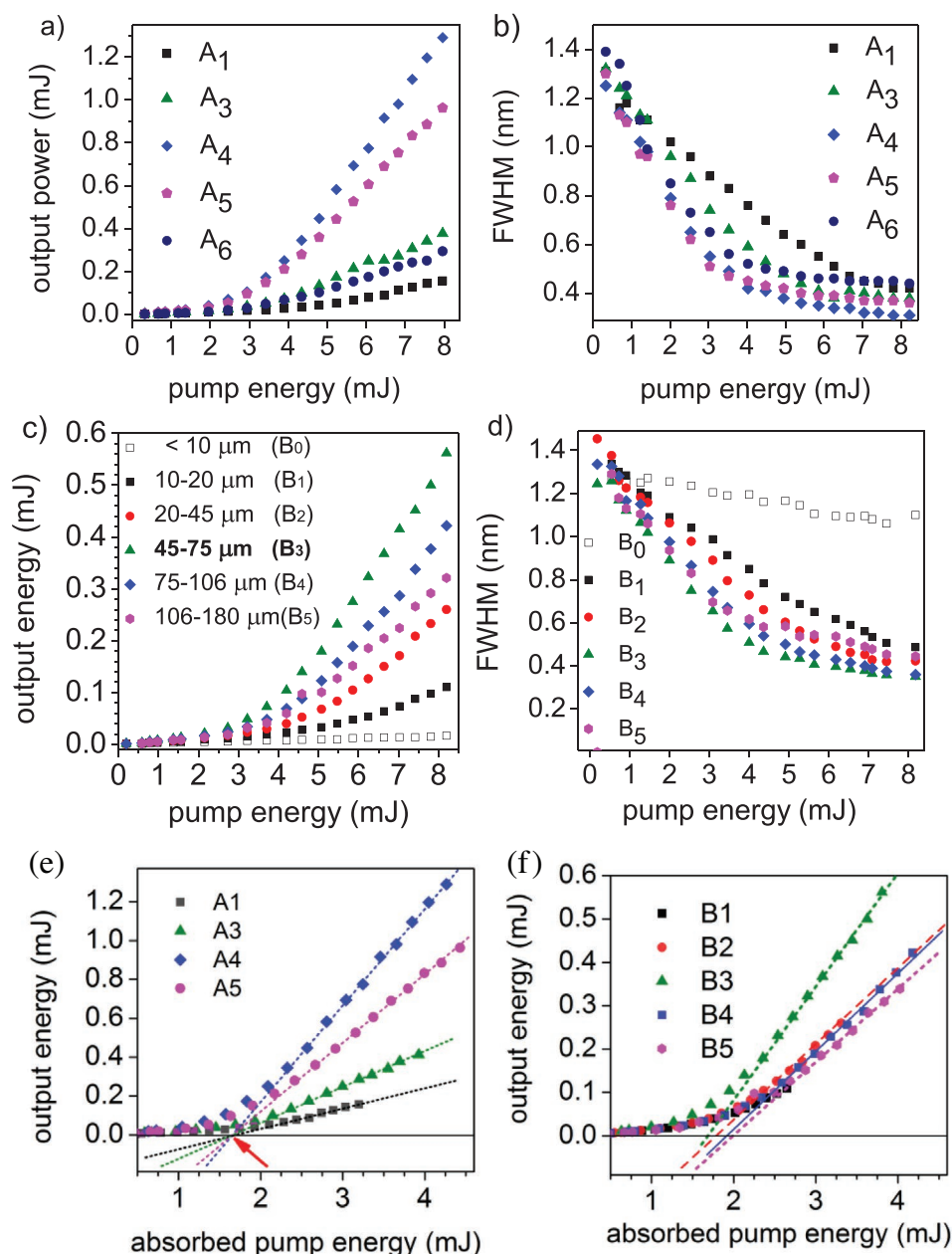
For spectroscopic measurements, the detector was substituted by a fiber-coupled spectrometer carefully aligned to the peak of the backscattering cone. The emission spectrum always consisted of one single peak and no other peaks or spikes were detected in any of the samples with our spectrometer of 0.1 nm resolution (see Figure S2, Supporting Information).

The part of the emitted radiation captured by the lens represents only a small fraction of the total power emitted by the random laser. Assuming a Lambertian emission, the total output power from the pellet is $(d/r)^2$ times bigger, where d is the distance to the lens (35 mm) and r is its useful aperture radius (11.2 mm), which in our case amounts to a 9.8 times higher output.[15] The total calculated output energy as a function of pump energy for the polydispersed samples is shown in **Figure 5**a.

The best performance for the A group is achieved with sample A_4. Its output energy is a factor eight times higher than for sample A_1. In order to show that the trend of decaying output power as a function of average grain size for particles bigger than A_4 is a continuing one, an additional pellet was fabricated, A_6, with the remains of the powder contained in the first sieve of 180 µm mesh size (particles > 180 µm). The average particle size for group A_6 was 278 µm as measured from SEM images. As expected, the output energy for samples A_6 is even smaller than for samples A_5. Figure 5b shows the linewidth narrowing of the polydispersed samples. The samples with the highest output energy show also the fastest linewidth narrowing, which is sample A_4 (average size of 54 µm). In Figure 5c,d, the results for the monodispersed groups B are shown. Sample B_3 (average size of 55 µm, triangles) showed the best laser performance, resulting in the highest output power (Figure 5c) and strongest linewidth narrowing (Figure 5d). When compared to sample B_1, the output power of sample B_3 is a factor five times higher. For comparison purposes, the highest emission intensity for $NdSc_3(BO_3)_4$ samples was achieved for a particle size of $\approx$10 µm.[30]

We investigated if lasing was possible even for powders of very small grain size and introduced one additional sample group, samples B_0, where we used the remains of the cleansed powders that passed through all sieves, inclusively the last sieve of mesh 10 µm. This was only possible because the washing procedure generated enough material of such small grain size. As expected this sample did not show any laser action, even at the maximum peak pump power of 55 W.[37] The behavior can be observed in Figure 5d (open squares) where group B_0 shows a linear and not an exponential decay. Figure 5e,f show the output energy as a function of the absorbed pump energy for the polydispersed and monodispersed groups, respectively. The slope efficiencies (dotted lines), determined by linear fittings, are displayed for each group (except for group B_1 that barely reaches linear gain and cannot be well fitted for this reason).

ADVANCED
SCIENCE NEWS
www.advancedsciencenews.com

Particle
& Particle Systems Characterization
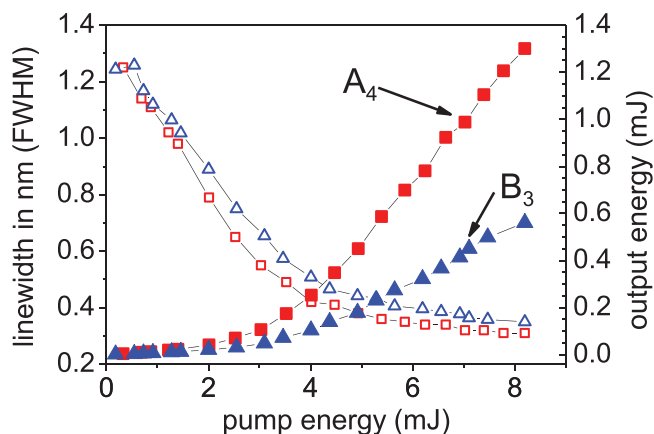www.particle-journal.com

Figure 5. a) Output energy as function of incident pump energy and b) linewidth narrowing as function of pump energy for polydispersed samples A. Group A_2 not shown because of overlap with A_3. c) Output energy as function of pump energy and d) linewidth narrowing as function of pump energy for monodispersed samples B. Output energy as a function of absorbed pump power for e) polydispersed and f) monodispersed samples. Shown are also the fitted slope efficiencies (dotted lines) for each group.

Clearly seen is that the polydispersed groups absorb more pump energy than the respective monodispersed groups, which is one of the central results of this work. Even more interesting is the fact that polydispersed groups all present a similar laser threshold, as shown by the arrow in Figure 5e. This last result supports the idea that the gain centers of the polydispersed samples are the pockets containing smaller particles. These pockets, present in all polydispersed samples (as demonstrated by Figure S1, Supporting Information), must be the place were laser oscillation starts. Owing to the light scattering being governed by the bigger particles, these pockets must be pumped

from all sides and from any direction, which does increase the efficiency of pumping.

Figure 6 shows a comparison between the most efficient samples of groups A and B. The best laser performance of each group occurs for similar mean grain sizes for the polydispersed and monodispersed powders of 54 µm (group A_4) and 55 µm (group B_3). Sample A_4 shows ≈2.3 times higher output energy when compared to sample B_3. This demonstrates clearly that the better performance of A_4 is due to its composite structure and cannot be achieved by means of a monodispersed sample. When comparing samples A_4 to samples B_4, which are both

**ADVANCED
SCIENCE NEWS**
www.advancedsciencenews.com

Particle
& Particle Systems Characterization
www.particle-journal.com

Figure 6. Comparison between the best samples from groups A (A$_4$) and B (B$_3$). Shown are linewidth narrowing (left axis) and laser output power (right axis).

obtained from the same mesh grids except that B$_4$ is cleansed, the difference in output power is a factor of 3.1.

The overall highest output power was achieved with sample A$_4$. With a pump pulse energy of 8.2 mJ at the pellet location, we achieved a total calculated output energy of 1.29 mJ at 1064 nm.

5. Discussion

From the reflection–absorption measurements with the integrating sphere we calculated a value of 41.7% absorbed power at the 806 nm incident pump radiation for the pellets of sample A$_4$ (including reflection in the first surface, Fresnel losses). Therefore, the optical efficiency in terms of absorbed pump power is 34% with a corresponding slope efficiency of 50%. This slope efficiency is comparable to diode pumped bulk-Nd:YVO$_4$ lasers! The slope efficiency of a laser, σ_S, is the product of the input coupling efficiency (η_{IC}) and the output coupling efficiency (η_{OC}), $\sigma_S = \eta_{IC} * \eta_{OC}$. The input coupling efficiency itself is the product of several other efficiencies. Amongst those is the absorption efficiency, η_{abs}, that is approximately

$$\eta_{abs} \approx T\left[1 - 1/\text{FAP}\right] = T\left[1 - \exp\left(-l_c/l_a\right)\right] \quad (3)$$

where T is the sample surface transmission and FAP values are shown in Table 2 for a monochromator with a resolution of 0.2 nm. In our laser experiment however, we use a qcw diode laser of 2.8 nm width (measured FWHM). We calculated the spectral overlap integral between the spectrum of the pellet (sample A$_4$, Figure 3a) and the diode's spectrum at 806 nm and, as a result, the effective microscopic absorption length increases by 27%. For comparison, our OPO (Opolette, COHERENT Inc.) has a linewidth (FWHM) of 0.7 nm at 806 nm, which would result in an absorption length increase of mere 2.2% with respect to the monochromator. Therefore, when comparing the absorption efficiency of a diode-pumped system with an OPO pumped system we calculate an increase for the OPO pumped system of 16%, resulting in a slope efficiency of 58%. The results are shown in **Figure 7**a and demonstrate that these powder random lasers can be efficiently pumped by diode lasers without large loss in output efficiency.

At very low pump powers, the total, spectrally integrated output power of the samples depends linearly on the absorbed pump power. This output signal originates from a sample volume given by the numerical aperture of the collecting lens (which in our case is the same as the focusing lens), Figure 4b given by area A and depth of volume d_0. We noted that at the lowest pump power of 0.3 mJ the average spectrally integrated output power is almost constant amongst the samples of groups A and B to within less than 5%. We therefore approximate the output power at low pump powers, I_{LP}, by

$$I_{LP} = C * \text{ff} * l_S * \left(1 - e^{\frac{d_0}{l_S}}\right) \quad (4)$$

If we further assume that $l_S \approx l_T$, where l_T are the values obtained from the backscattering cone measurements, and calculate $d_0 = 6$ μm given the pump focusing setup described above, we obtain the constant C in Equation (4) by fitting the formula to the fill fraction values ff* calculated in Table 2 from the particle distributions. We can now calculate the missing fill
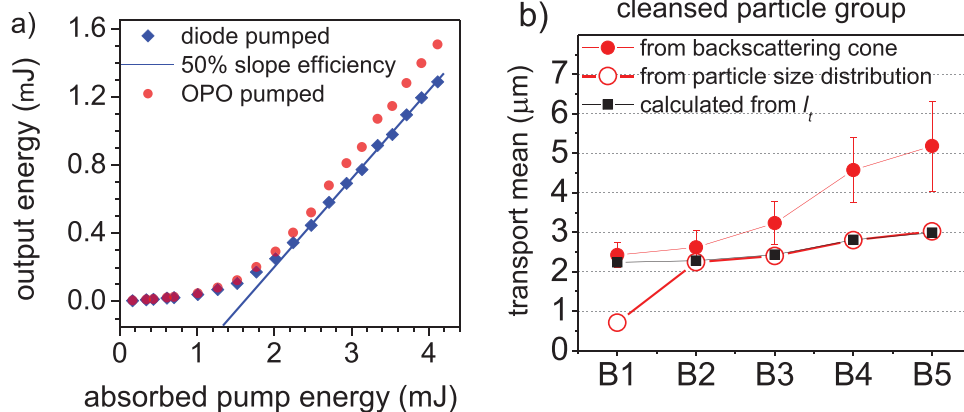
Figure 7. a) Comparison of output power as a function of absorbed pump power for diode pumping and OPO pumping. b) Measured transport mean free path for groups B (filled circles) and calculated values from particle size distribution (open circles) and using Equation (4) (squares).

**ADVANCED
SCIENCE NEWS**

www.advancedsciencenews.com

Particle
& Particle Systems Characterization

www.particle-journal.com

Table 3. Calculation of the mean photon path length l_C for backscattering using Equation (1) and values for the fill fraction from Table 2.

Polydispersed l_c		Monodispersed l_c	
A_1	154 μm	B_1	127 μm
A_2	193 μm	B_2	180 μm
A_3	251 μm	B_3	255 μm
A_4	343 μm	B_4	357 μm
A_5	406 μm	B_5	360 μm

fractions for groups B_1, A_1, A_2, and A_3 (ff** in Table 2). The results are shown in Figure 7b.

It is known that random close packing of monodispersed spheres results in 63% volume fill fraction. This value is lower than for organized packing, which results in higher filling fractions (for example, hexagonal close packing of spheres results in 74% filling fraction).[38] If the particles are still monodispersed but present more irregular shapes, for example ellipsoids, then random close packing may result in different values for the fill fractions depending upon shape, for example, 0.74 for certain ellipsoids.[39] These values compare roughly with our results from the more monodispersed groups B_4 and B_5, but also A_5, that show on average a fill fraction of 0.62.

If the particles are polydispersed, such as in samples A_1 to A_3, then the volume fraction depends nontrivially on the size distribution and can be arbitrarily close to one. The smaller particles that are present in groups A_4 down to A_1 gradually fill up the voids between the larger particles and increase the fill fraction. As voids become more and more filled up, the smaller particles overcome the repulsive coulomb forces and start to touch each other, building agglomerates.[40,41] For interparticle distances less than one wavelength, the agglomerate must behave as a bigger particle with a lower effective refractive index and scattering cross-sections. These effects together, smaller effective scattering cross-section, smaller effective refractive index, and several particles together behaving like a single large particle (agglomerate), work in the direction of increasing l_t of groups A_1, A_2, A_3, and B_1 as shown in Figure 3. Next we can calculate the mean photon path length l_C. The results are shown in **Table 3**.

Similar values of l_C are observed in both groups. This indicates that the bigger particles, which are common to both groups, are the principal responsible for the macroscopic distribution of light within the samples. Additionally, as explained before, l_t values of polydispersed samples (A) are lower than those for monodispersed samples (B), indicating a higher quantity of scattering events for polydispersed samples (**Figure 8**a).

The gain coefficient in Nd (1.33 mol%):YVO_4 for unpolarized light is $\gamma = 127$ cm^{-1}.[29] Given the fill fractions of groups B_3 and A_4 (see Table 2) and the mean photon path lengths, l_c, (Table 3) we may calculate the ratio of the gains of both groups

$$\frac{e^{\gamma * \text{ff}_{A_4} * l_{CA_4}}}{e^{\gamma * \text{ff}_{B_3} * l_{CB_3}}} = 1.65 \tag{5}$$

and compare to the ratio of the slope efficiencies measured in Figure 6, which is 1.75 when plotted as a function of absorbed pump power. We therefore have a good agreement between relative output power, measured directly using a power meter, and results obtained using measurements from backscattering cone and reflection-absorption experiments. This also reveals that the FAP measurement is a promising technique for studying the diffusion of light in a scattering medium.

The number of scattering events undergone by backscattered photons is shown in Figure 8a. The best performing groups of the monodispersed and polydispersed samples, B_3 and A_4, respectively (see Figure 6), also show the highest ratio of l_c/l_t. On average, samples from A groups undergo 15% more scattering events than the corresponding monodispersed samples from B groups, however, l_c values are approximately equal (Table 3). Therefore the density of absorbed energy in the A groups should also be ≈15% bigger when compared to the corresponding B group. This increase must be due to the additional absorption provided by the particles trapped in the space between the larger particles of the polydispersed group. If we compare the fill fraction of A with B in Table 2, we see that groups A have on average a 2% higher fill fraction due to additional small particles. Therefore, the additional 15% absorbed energy is located mainly within the pockets containing 2% of smaller particles. If we take, for example, sample A_4 which has a fill fraction of 0.66, this means that the absorbed energy in the pockets would be five times higher than in the bigger particles.
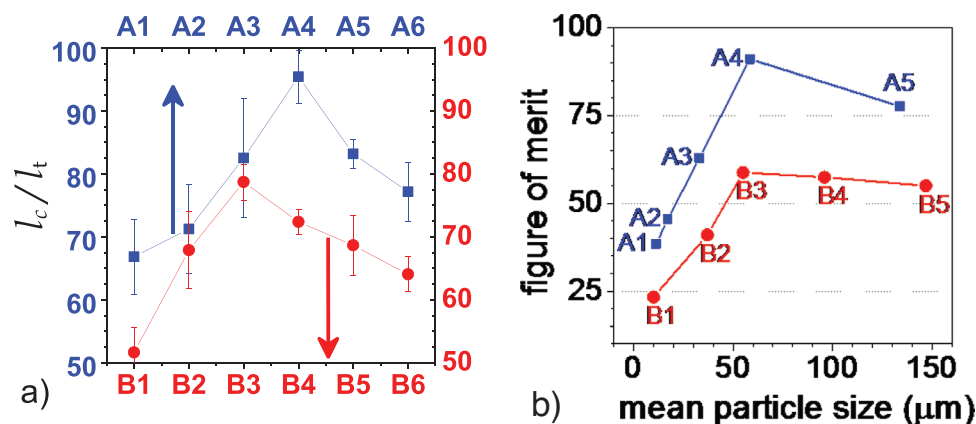
Figure 8. a) Comparison between numbers of scattering events experienced by pump photons. b) Figure of merit of both groups.

**ADVANCED
SCIENCE NEWS**
www.advancedsciencenews.com

Particle
& Particle Systems Characterization
www.particle-journal.com

A figure of merit can be established composed of the absorbed energy ($l_C * ff / l_a$, Equation (1)) times the density factor (l_C / l_t). If we compare these calculations, shown in Figure 8b, with the laser output power results of Figure 5, we observe a good qualitative agreement: for example, A_5 shows more output power than B_3 that is similar to A_3.

Finally, other crystalline materials with high index of refraction and high emission cross-section could be used instead of $Nd:YVO_4$ such as $Nd:GdVO_4$ or $Nd:Sc_2O_3$ and should present similar results upon using polydispersed compositions. We also tried materials based on binary glasses containing heavy metal oxides that are responsible for a high index of refraction and that can be highly doped, but without success.[42]

6. Conclusion

Pressed pellets of $Nd^{3+}:YVO_4$ powder have been prepared and optimized in terms of grain size distributions. Using polydispersed powder mixtures, we achieved an increase of 130% (2.3x) in output power, with respect to the best monodisperse powder (comparison of A_4 and B_3). In direct comparison, the effect of the smaller particles is an increase of $3.1\times$ in terms of output power (comparison of A_4 and B_4). Maximum output pulse energy of 1.3 mJ was achieved with a slope efficiency of 50% as a function of absorbed pump power, demonstrating that these random lasers can be efficiently pumped by semiconductor diodes. Additionally a slope efficiency of 58% is calculated for OPO pumping. For all polydisperse samples, a similar random laser threshold is observed, which was attributed to that the pockets determine the threshold and these are similar for all samples.

We have shown that the light diffusion is governed mainly by the larger particles and it is almost independent of the smaller particles. The smaller particles, which are trapped between the larger particles, are responsible for an increase of 15% in the number scattering events, increasing the local pump power density (increase of five times for group A_4). Therefore, these pockets of smaller particles can be envisioned as absorption and gain centers. In addition to their optical properties (l_t, volume), these pockets are pumped by all sides and from any direction. This strategy of using smaller particles to fill the spaces between the larger particles opens a new way to increase the efficiency of random lasers. A promising technique (FAP) allowed us to characterize light diffusion and efficiency of the random laser. The FAP characterization and associated parameters such as l_c and l_c/l_t give valuable information on the random laser performance and increases the insight on how light diffusion and pump absorption behave in the detail.

Supporting Information

Supporting Information is available from the Wiley Online Library or from the author.

Acknowledgements

Conflict of Interest

The authors declare no conflict of interest.

Keywords

[1] V. S. Letokhov, *JETP Lett.* **1967**, *5*, 212.
[2] V. S. Letokhov, *Sov. Phys. JETP* **1968**, *26*, 835.
[3] C. Gouedard, D. Husson, C. Sauteret, F. Auzel, A. Mingus, *J. Opt. Soc. Am. B* **1993**, *10*, 2358.
[4] H. Cao, Y. G. Zhao, S. T. Ho, E. W. Seelig, Q. H. Wang, R. P. H. Chang, *Phys. Rev. Lett.* **1999**, *82*, 2278.
[5] R. C. Polson, A. Chipouline, Z. V. Vardeny, *Adv. Mater.* **2001**, *13*, 760.
[6] R. C. Polson, Z. V. Vardeny, *Appl. Phys. Lett.* **2004**, *85*, 1289.
[7] D. S. Wiersma, *Nat. Phys.* **2008**, *4*, 359.
[8] K. C. Jorge, M. A. Alvarado, E. G. Melo, M. N. P. Carreño, M. I. Alayo, N. U. Wetter, *Appl. Opt.* **2016**, *55*, 5393.
[9] B. Redding, M. A. Choma, H. Cao, *Nat. Photonics* **2012**, *6*, 355.
[10] Z. Wang, H. Wu, M. Fan, L. Zhang, Y. Rao, W. Zhang, X. Jia, *IEEE J. Sel. Top. Quantum Electron.* **2015**, *21*, 10.
[11] H. Watanabe, Y. Oki, M. Maeda, T. Omatsu, *Appl. Phys. Lett.* **2009**, *86*, 151123.
[12] M. Bahoura, K. J. Morris, G. Zhu, M. A. Noginov, *IEEE J. Quantum Electron.* **2005**, *41*, 677.
[13] M. A. Noginov, N. Noginova, S. U. Egarievwe, H. J. Caulfield, C. Cochrane, J. C. Wang, M. R. Kokta, J. Paitz, *Opt. Mater.* **1998**, *10*, 297.
[14] M. A. Noginov, I. N. Fowlkes, G. Zhu, *Appl. Phys. Lett.* **2005**, *86*, 161105.
[15] J. Azkargorta, I. Iparraguirre, M. Barredo-Zuriarrain, S. García-Revilla, R. Balda, J. Fernández, *Materials* **2016**, *9*, 369.
[16] I. Iparraguirre, J. Azkargorta, K. Kamada, A. Yoshikawa, U. R. Rodríguez-Mendoza, V. Lavín, M. Barredo-Zuriarrain, R. Balda, J. Fernández, *Laser Phys. Lett.* **2016**, *13*, 035402.
[17] M. A. Noginov, N. E. Noginova, S. U. Egarievwe, H. J. Caulfield, P. Venkateswarlu, A. Williams, S. B. Mirov, *J. Opt. Soc. Am. B* **1997**, *14*, 2153.
[18] R. J. R. Vieira, L. Gomes, J. R. Martinelli, N. U. Wetter, *Opt. Express* **2012**, *20*, 12487.
[19] Z. Shang, M. Yang, L. Deng, *Materials* **2016**, *9*, 725.
[20] A. Espinha, M. C. Serrano, A. Blanco, C. López, *Adv. Opt. Mater.* **2015**, *3*, 1080.
[21] A. L. Moura, L. J. Q. Maia, A. S. L. Gomes, C. B. de Araújo, *Opt. Mater.* **2016**, *62*, 593.
[22] E. Jimenez-Villar, V. Mestre, P. C. Oliveira, G. F. de Sá, *Nanoscale* **2013**, *5*, 12512.
[23] E. Jimenez-Villar, V. Mestre, P. C. Oliveira, W. M. Faustino, D. S. Silva, G. F. Sá, *Appl. Phys. Lett.* **2014**, *104*, 081909.
[24] E. Jimenez-Villar, I. F. da Silva, V. Mestre, P. C. Oliveira, W. M. Faustino, G. F. Sá, *Nanoscale* **2016**, *8*, 10938.

[25] E. Jimenez-Villar, I. F. da Silva, N. U. Wetter, C. Lopez, V. Mestre, P. C. Oliveira, W. M. Faustino, G. F. Sá, *ACS Omega* **2017**, *2*, 2415.

[26] N. U. Wetter, F. A. Camargo, E. C. Sousa, *J. Opt. A: Pure Appl. Opt.* **2008**, *10*, 104012.

[27] N. U. Wetter, E. C. Sousa, F. A. Camargo, I. M. Ranieri, S. L. Baldochi, *Opt. Laser Technol.* **2017**, *96*, 271.

[28] N. U. Wetter, E. C. Sousa, F. A. Camargo, I. M. Ranieri, S. L. Baldochi, *J. Opt. A: Pure Appl. Opt.* **2008**, *10*, 104013.

[29] M. Schmidt, E. Heumann, C. Czeranowsky, G. Huber, in *Advanced Solid-State Lasers* (Ed: C. Marshall), OSA Trends in Optics and Photonics Series, Vol. *50*, Optical Society of America, Washington DC, USA **2001**, p. 470.

[30] J. M. Giehl, A. R. Miranda, S. M. Reijn, F. Butzbach, N. U. Wetter, in *Advanced Solid State Lasers, OSA Technical Digest*, Optical Society of America, Washington DC, USA **2014**, p. 114829.

[31] J. M. Giehl, F. Butzbach, K. C. Jorge, M. A. Alvarado, M. N. P. Carreño, M. I. Alayo, N. U. Wetter, *Proc. SPIE* **2016**, *9893*, 989314.

[32] E. Akkermans, P. E. Wolf, R. Maynard, *Phys. Rev. Lett.* **1986**, *56*, 1471.

[33] M. Bahoura, M. A. Noginov, *J. Opt. Soc. Am. B* **2003**, *20*, 2389.

[34] M. B. van der Mark, M. P. van Albada, A. Lagendijk, *Phys. Rev. B* **1988**, *37*, 3575.

[35] A. Lagendijk, R. Vreeker, P. De Vries, *Phys. Lett. A* **1989**, *136*, 81.

[36] S. E. Skipetrov, I. M. Sokolov, *Phys. Rev. Lett.* **2014**, *112*, 023905.

[37] M. A. Noginov, G. Zhu, A. A. Frantz, J. Novak, S. N. Williams, I. Fowlkes, *J. Opt. Soc. Am. B* **2004**, *21*, 191.

[38] C. Song, P. Wang, H. A. Makse, *Nature* **2008**, *453*, 629.

[39] A. Donev, I. Cisse, D. Sachs, E. A. Variano, F. H. Stillinger, R. Connelly, S. Torquato, P. M. Chaikin, *Science* **2004**, *303*, 990.

[40] O. L. Sánchez-Muñoz, J. Salgado, J. Martínez-Pastor, E. Jiménez-Villar, *Nanosci. Nanotechnol.* **2012**, *2*, 1.

[41] G. Fuertes, O. L. Sánchez-Muñoz, E. Pedrueza, K. Abderrafi, J. Salgado, E. Jiménez, *Langmuir* **2011**, *27*, 2826.

[42] T. A. A. de Assumpção, L. R. P. Kassab, A. S. L. Gomes, C. B. de Araújo, N. U. Wetter, *Appl. Phys. B* **2011**, *103*, 165.